

INVESTIGATION INTO THE SPATIO-TEMPORAL PROPERTIES OF ARCS IN VACUUM ARC REMELTING FURNACES

Matthew Cibula¹, Rigel Woodside¹, Paul King¹, Gordon Alanko²

¹Ampere Scientific; 33827 SE Eastgate Circle; Corvallis, OR 97330, USA

²ATI Specialty Alloys & Components; 1600 Old Salem Rd. NE, Albany, OR 97321, USA

Keywords: Vacuum arc remelting, electro-slag remelting, solidification, segregation, electric arc, side-arc, magnetic tomography, arc location

Abstract

The behavior of vacuum arcs during VAR processing is known to impact product yield and contribute to ingot defects. Ampere Scientific's *VARmetric*TM system has demonstrated non-invasive detection of the spatio-temporal properties of vacuum arcs, including the detection of side-arcing conditions, by utilizing measurements of the magnetic field external to the furnace.

Here we present an analysis of spatio-temporal arc distributions measured by *VARmetric*TM on a production VAR furnace. Analysis of the arc over different timescales provides new insights into the operating characteristics of VAR furnaces, and on how power is transferred to the molten pool. For example, even under similar steady state operating conditions within a given melt, we have identified significantly different arc distributions, information that may be useful in further understanding the characteristics of the molten metal pool.

Introduction

Vacuum Arc Remelting (VAR) is a key step in the production of specialty metals and alloys that increases homogeneity and reduces defects in the remelted ingot. VAR is frequently used with Ni- and Ti- based alloys for high-performance applications, including aerospace rotating systems. In this process, the input material (electrode) is gravity fed into a water-cooled crucible within a vacuum chamber, with melting energy provided by a vacuum arc that is sustained between the electrode and the output material (ingot). The heating from the vacuum arc causes molten material to drip off the electrode tip into the molten portion of the ingot.

In most furnaces, the quality of the metals produced by VAR furnaces and the safety of the remelting process are controlled to the extent that is possible with real-time process measurements. The current, voltage, and vacuum pressure are controlled to follow a designated "melt profile" with a fixed melt rate. Melt rate control is commonly applied with a ramp up time at the beginning of the melt, a 'steady-state' period, and a low power period at the end of the melt. The melt rate is usually controlled by the current input to the furnace with feedback from a load cell that monitors the weight of the electrode. The voltage across the furnace and measurement of the 'drip-short' frequency may be used to monitor the size of the gap between the electrode and the ingot [1]. While the process measurements can provide a standard baseline from which to compare different melts, they do not provide enough information to accurately predict solidification-related defects in the forming ingot.

Furthermore, these standard process measurements are unable to detect side-arcs in real-time. Side-arcs are a safety-critical condition during VAR due to the high reactivity of the processed

materials and the large amount of energy applied. Most furnaces are equipped with video cameras to monitor the annulus between the electrode outer wall and the crucible inner wall, and operators monitor the annulus during melting for side-arcs. A stirring coil is commonly applied, which generates axial magnetic fields that are thought to confine arcs to the bottom of the electrode and induce stirring in the molten pool. These approaches are still not completely effective in preventing or reacting to side-arcs.

The discussion of these problems and the presented work requires a clear definition of the vacuum arc. The arc is the total electrical discharge between the electrode (cathode) and the ingot (anode), and is sustained by a metal vapor plasma formed by the vaporization and ionization of the electrode. Discrete cathode spots constitute the main current transfer mechanism, while a lesser diffuse current transfer is associated with the plasma. The cathode spots provide concentrated joule heating to the electrode in an area of 10-100 μm with current densities around 10^9 A/m^2 , and carry approximately 70 A per spot depending on the material [2]. For a furnace operating above 10 kA, there may be over 100 simultaneous cathode spots. These spots may group together into clusters, which have been observed to carry 380 Amps within a 3cm diameter, but at any given instant the cathode spots and groups only cover a small portion of the electrode [3]. While this arc distribution is non-uniform and composed of discrete cathode spots instantaneously, the distribution is continuous over longer time periods and is commonly found in a diffuse or constricted mode. Constricted arcs were linked to the formation of material defects in nickel alloys, but the preferential mode of arcing may depend on the material and furnace properties [4].

To enhance VAR process monitoring, Arc Position Sensing (APS) technology was developed at the National Energy Technology Laboratory (NETL) with funding provided by the Specialty Metals Processing Consortium (SMPC) [5]. Because there are multiple sources, the single-arc method of APS locates the centroid of the arc distribution rather than the locations of individual cathode spots or cathode spot groups [6]. This technology is now commercialized in Ampere Scientific's *VARmetric*TM system. The system is non-invasively attached to a VAR furnace and determines the position of the arc centroid in real time. Additionally, the information obtained can be used to approximate the power input to the ingot during VAR to assess melt profiles, for example, as a solidification modeling input. Previously reported results have shown notable variations in ingot side wall solidification rates due to observed variations in the arc distribution [7]. We also show that the measurements provide a mechanism to monitor the furnace for side-arcing conditions.

Methodology

The non-invasive arc position sensing is based on the relationship between current density and magnetic flux density vectors as described in equation 1, the Maxwell-Ampere Law.

$$\nabla \times \vec{B} = \mu \left[\vec{J} + \frac{\partial \vec{D}}{\partial t} \right], \quad (1)$$

where the arcs are considered current sources, \vec{J} , which exist inside the furnace and magnetic flux density vectors, \vec{B} , are measured at a distance outside of the furnace. As can be seen in equation 1, the relationship between current and magnetic fields also depends on the magnetic permeability of the medium, μ , and a time varying electric displacement, $\frac{\partial \vec{D}}{\partial t}$. VAR furnaces are typically constructed of materials having a relative permeability of 1, simplifying the solutions to equation 1. VAR furnaces are also usually DC powered so time varying electric fields can be neglected. Finally, since our interest is at the relatively slow time scales of melting and solidification, the arc can be considered as being stationary at an instant in time. This last assumption is almost certainly violated by an individual cathode spot. However, the average of several cathode spots, an arc centroid, will tend to produce slowly varying magnetic fields outside of the furnace, as has previously been reported [8]. To solve equation 1, the Finite Element Method (FEM) is utilized. A 3D CAD of the furnace is generated which considers the furnace's physical geometry, namely the crucible and electrode dimensions and the positions of the sensors relative to those components. In the FEM modeling, possible arc locations and ingot heights are simulated to generate a database of expected magnetic fields as they relate to defined furnace states. The number of furnace states to consider depends on the details of the furnace, but in general the number of computations required can be greatly reduced by considering principles of symmetry and superposition. Still, running a FEM model is not computationally practical for real time VAR application, so a reduced order model is implemented. The reduced order model is based on equation 2, the Biot-Savart Law.

$$\vec{B}(\vec{r}) = \frac{\mu_0}{4\pi} \int \frac{Id\vec{l} \times \vec{r}}{|\vec{r}|^3}, \quad (2)$$

where $\vec{B}(\vec{r})$ is the magnetic field vector at point in space, representing a sensing point, and the arc is a line source of current carrying I amps. The \vec{r} represents a distance vector from the source to the sensing point. μ is the permeability in vacuum, which has a relative permeability of 1. The equations can be further reduced and generalized via some parameters by considering only a single arc and treating the arcs as straight line sources pointed in the axial direction within the arc gap. The resulting two equations for the tangential (B_t) and radial (B_ρ) components of the magnetic field in the polar coordinate system are shown in equations 3 and 4.

$$B_\rho = m_r I \left(\frac{\sin(\theta)}{d} - a \right), \quad (3)$$

$$B_t = m_t I \left(\frac{\cos(\theta)}{d} - b \right). \quad (4)$$

The location of the arc and the locations of the sensors are both input to the FEM modeling, which solves for the magnetic fields at the sensing points, and the results are then used to determine the coefficients, m_ρ , m_t , a , and b for each sensor. The inverted forms of these equations are then applied in APS to calculate arc locations in the furnace during melting. This parameter based estimation approach is referred to as the single arc method, and the arcs can be deterministically located on the electrode surface, as shown by the red dot in figure 1. This may also represent the centroid of multiple arcs centered around this point, as shown by the dotted red line in figure 1. There are some errors associated with parametrizing the system, but these errors tend to be small, and are also systematic

such that corrections can be made [9]. The APS technology utilized is exclusively licensed to Ampere Scientific as part of NETL's electric current locator IP. Notably, the technique also applies to the location of any number of arcs using a superposition based form of equations 3 and 4 and multiple sensing points. The interest in this study is the arc distribution for the overall melt profile, and we show the single arc method provides a convenient means of analyzing this. Locating multiple arcs in real time is under development, and can be expected to provide more accurate arc distributions at shorter time scales than evaluated in this study.

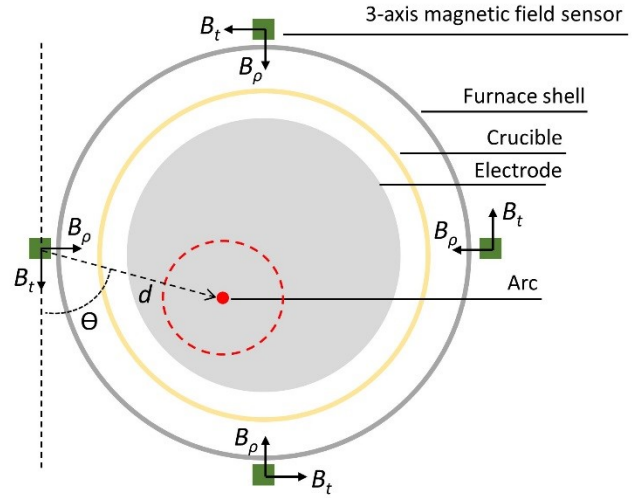


Figure 1 – Model for Arc Position Sensing. Four sensors on the exterior of the furnace measure the magnetic fields generated by the arcs, centered at the red dot and located within the red dotted line.

In order for the arc to be located with just two components of the magnetic field, the location of the electrode gap must be known. This is estimated using existing melt rate data and ram position data. While the vertical component of the magnetic field, $B_z(z)$, contains information about the vertical location of the arc in the furnace relative to the sensor, it is also strongly influenced by the details of side wall currents. With this consideration, B_z is not used in arc position sensing in order to avoid any dependence on assumptions made about the side wall current. However, B_z fields are still useful in determining the existence of side-arcs in the furnace, where an arc transfers current directly between the electrode and the crucible wall, rather than traveling through the ingot. Notably, if the arc gap between the electrode tip and the ingot is aligned with sensor, $B_z^{AG}(z=0) = 0$ regardless of arc motion within the gap; however, the sensors may be located above or below the arc gap where this term is non-zero. The addition of a side-arc above this plane introduces a new component to the magnetic field, B_z^{SA} , that is non-zero in the plane so by superposition, $B_z(z) = B_z^{AG}(z_1) + B_z^{SA}(z_2)$, where $z_2 > z_1$. B_z^{SA} also depends on the angular location of the sensor relative to the side-arc, θ , so that by measuring B_z with a ring of sensors, side-arcs generate a distinct change that can be separated from the magnetic field generated by arcs within the arc gap, B_z^{AG} . Thus, side arc detection works by flagging changes in the B_z field patterns over short time durations.

A VARmetric™ measurement system was deployed on a production-scale VAR furnace at ATI Specialty Alloys &

Components for a series of melts, including three different crucible sizes. Melts in the same crucible were subject to the same melt profile. The steady state melting was monitored by multiple rings of sensors to continuously locate the arc centroid. Figure 2 shows a picture of a sensing rings undergoing calibration, and attached sensing rings to a production VAR.



Figure 2 – Left: A single ring of the VARmetric™ measurement system undergoing calibration pre-installation. Right: VARmetric™ installed on a production furnace, with multiple rings to measure the arc as the ingot grows in the furnace.

The furnace current, voltage, ram position, and magnetic fields were sampled with VARmetric™ at 3 kHz and averaged down to 120 Hz for analysis. The ingot height throughout the melt is calculated using the ram position measurement, the size and density of the electrode, and the size of the crucible. A total of 6 melts are presented, with 2 melts in a 17” diameter crucible, 2 melts in a 20” diameter crucible, and 2 melts in a 23” diameter crucible.

The single arc method of APS also allows for an indirect approach to determine the diameter of the arc. This relies on the assumption that during the melt, the diameter of the arc must cover the full surface of the bottom of the electrode to transfer the electrode material into the molten ingot. The requirement is assumed to hold during the melt within a growth period for the ingot, which is limited by the extent of the concave or convex shape of the bottom of the electrode. We assume that this distance is approximately 1” for the melts presented here. The 90th percentile radius of the arc distribution centroid is used to set the arc diameter over each growth period, which is the difference between the radius of the electrode and the radius of the arc.

Results and Discussion

Figure 3 shows a direct comparison of the magnetic fields produced by the model and of those experimentally observed on the furnace, normalized by the current input to the system. The magnetic signal arising from the arc in the tangential and radial directions around the furnace is strongest at the plane of the sensor, but decreases away from the sensor. VARmetric™ uses multiple rings of sensors at different vertical planes to constantly measure the arc as the arc gap moves up the furnace. The magnetic fields measured by two

different sensors are shown, illustrating how the signal from the arc is overlapped. It is also clear that the experimental signals are notably weaker than those expected by the model. This is due to two main factors. First, it is expected that there are multiple arcs present, and the more arcs there are the more confined results for the single arc method will be in space. Second, the plasma current is generally more diffuse, yielding more centered distributions than expected by cathode spot current alone. Related to this phenomenon, prior studies have shown that nearly 50% of the input current may not travel into the ingot [10]. Under such conditions, in general, it is expected that the radial position of the determined arc location is slightly reduced, but the angle at which the arc is located is unaffected.

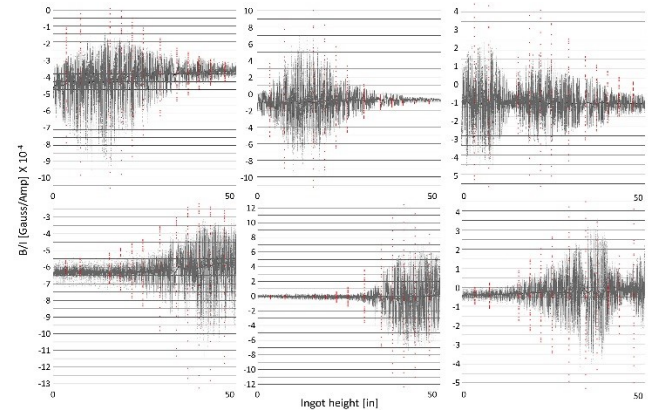


Figure 3 – Plots of the magnetic field normalized by the furnace current as a function of the ingot height during a melt for two magnetic field sensors, located at different heights outside the furnace.

The arc location was recorded over 31” within the steady state segment of the melt, constituting 31 1” growth periods over which the arc diameter was calculated. Two of these growth periods, 0” and 20” into the steady-state melt, were arbitrarily selected to present a sample of the arc distributions that were measured during these melts. For each crucible, two melts were selected to compare the arc distributions throughout the melt. Figure 4 shows the arc distributions for each type of crucible at the selected growth periods. The power input at the top of the ingot is found by including the arc diameter in the distribution and assuming the current is evenly distributed. This assumption is weakest when there are only a few arc columns, but holds well for diffuse arcs with many columns or a single constricted arc. Figure 5 shows the power input for each of the growth regions shown above. The distributions are primarily axis-symmetric, which is a good indicator that the growth period is large enough to accurately determine an average arc diameter. By binning this information across two orthogonal axes, it is possible to examine cross-sections of the power input to the ingot during the entire steady-state portion of the melt, shown in figure 6. These power profiles are a useful way to analyze the homogeneity of an ingot and pick out regions that may require closer inspection, since the input power is known to impact the solidification of the ingot.

In addition to the melts previously described, a controlled, short duration side-arc was tested during a melt to study the resulting magnetic field distribution and test side-arc detection. FEM simulations of an arc column across the gap between the electrode and crucible sidewalls were used to predict the magnetic field

strength at each sensor's location, B_Z^{SA} . The primary difference between the current path for a side-arc and that of an arc within the arc gap is that the side-arcing current is not significantly dispersed in the ingot as shown in figure 7. This difference disrupts the symmetry in the magnetic field, B_N , which can be detected by observing the changes in the fields over time.

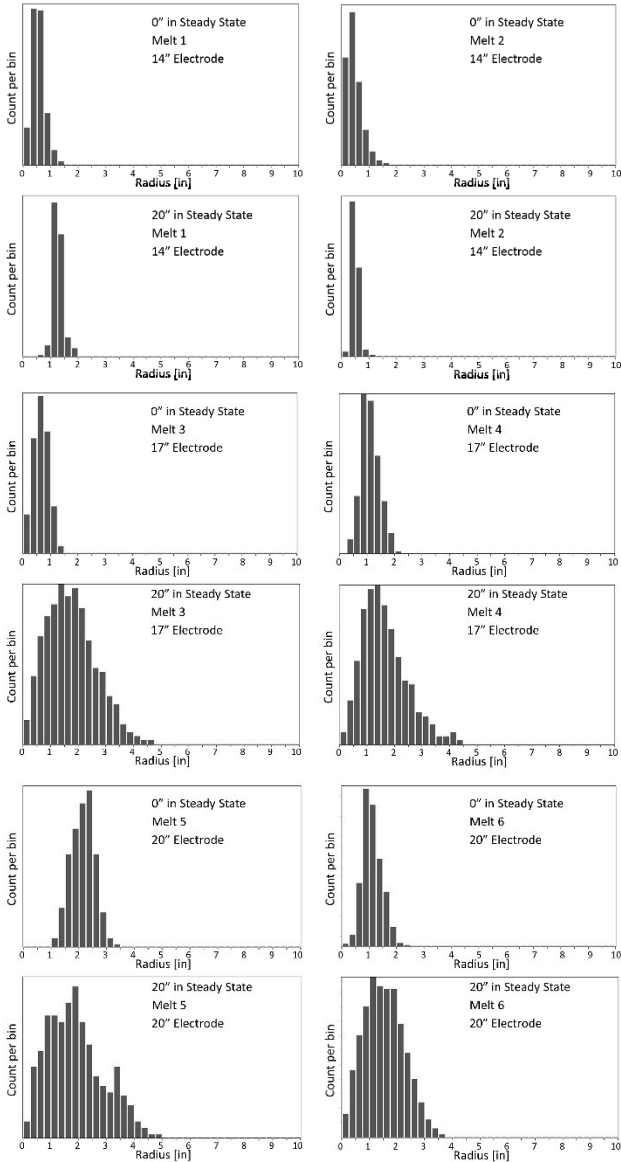


Figure 4: Histograms showing the centroid of the arc distribution during steady state melting. The data is binned in 0.25" segments in each growth period to profile the centroid distribution as a function of the radius from the center of the furnace.

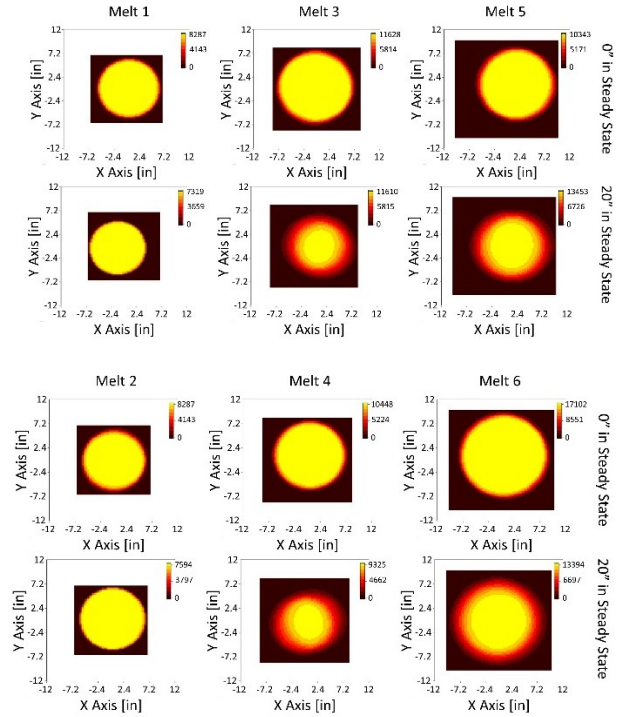


Figure 5: 2D distribution of the power input to the ingot over the growth periods. With the assumption that power is evenly distributed across the arc diameter, a uniform power density indicates a more diffuse arc, while non-uniform power density indicates more constriction.

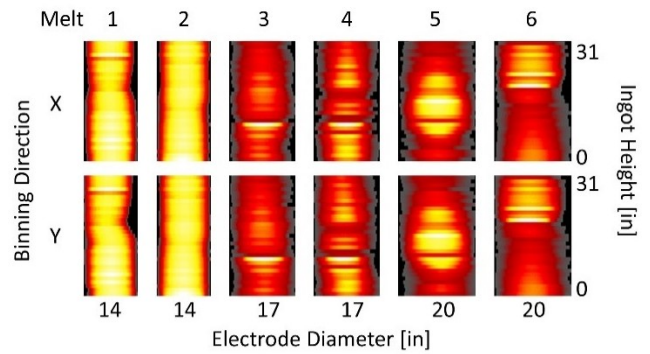


Figure 6: Cross-section of the power input to the ingot during the melt as a function of the ingot height (ingot power profile) for various electrode diameters and melts. Data is shown for 31" of steady state melting, although the final ingots and their steady state melting periods may be longer. The power input to the ingot depends on the spatio-temporal properties of the arc, rather than the assigned melt profile, so that melts with the same assigned melt profile may result in different ingot power profiles.

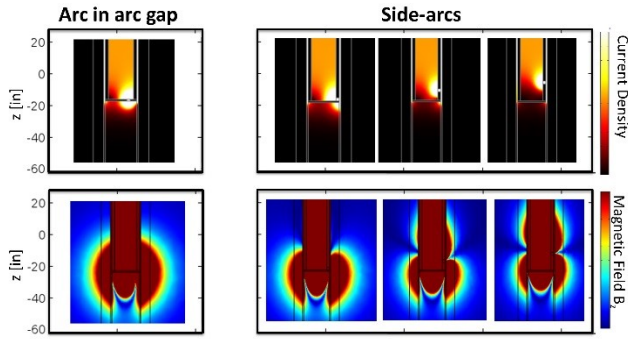


Figure 7: Simulated current density (top) and total magnetic field, B_N (bottom). Shown for arcs within the arc gap (left), and side-arcs at varying heights (0", 6", and 12") from the bottom of the electrode (right).

The magnetic fields, B_z^{SA} , were superimposed with the magnetic field from a single arc in the arc gap, B_z^{AG} according to equations 5 and 6:

$$I = (1 - \gamma)I^{AG} + \gamma I^{SA}, \quad (5)$$

$$B_z = B_z^{AG} + B_z^{SA}, \quad (6)$$

with the current proportion, γ , varied from 0% to 100%. The simulated magnetic fields were compared to the experimental measurements to determine the strength of the side-arc. The results, included in figure 8, indicate that the ratio of the side-arc current to the arc gap arc during the experiment was approximately 26%.

Although the simulations and experimental data were closely matched, there are multiple sources of error that impacted the results. First, it should be noted that APS could not be used to determine the location of arcs within the electrode gap during the side-arc event, since the side-arc affects the tangential and radial magnetic field components. Instead, the arc location was found by comparing the measured magnetic fields to the superposition of each simulated arc location within the electrode gap and the simulated side-arc. While this eliminates any error from APS affected by the side-arc, the assumption of a single arc beneath the electrode still introduces error that accounts for differences between the simulation and the experiment. This most strongly affects the data during the side-arc, since it is a short duration and the arc within the electrode gap was observed to oscillate across the electrode at this time. Additionally, it is not known how much diffuse current transfer between the electrode and the crucible continues to occur during a side-arc, so the side-arc may have contained less than 26% of the total furnace current.

Conclusions

As the primary mode of energy transfer in VAR, the arc and its spatio-temporal properties are significant when considering the safety of the process and quality control of the product. The *VARmetric*TM system was developed to improve these aspects of VAR, with APS to monitor the location and distribution of the arc and side-arc detection to monitor the furnace for safety-critical events. Results from a *VARmetric*TM system on a production furnace at ATI Specialty Alloys & Components show the potential for the system to qualify furnaces and ingots, develop new melt profiles, and monitor day-to-day furnace operations.

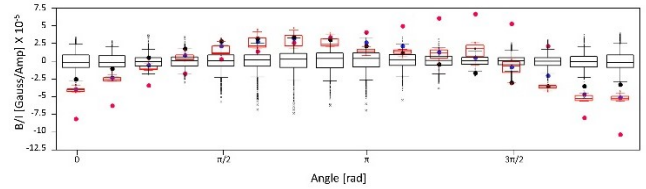
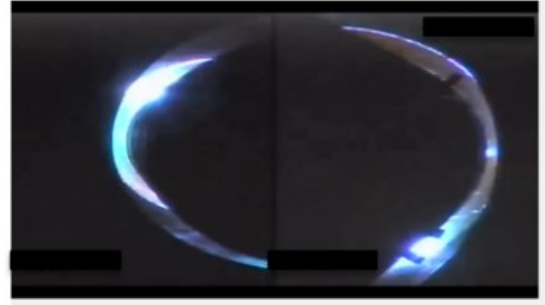


Figure 8: Results of the side-arc experiment. Top: image of the furnace annulus during the side-arc discharge. Bottom: 16 different sensors' measurement of B_z during (red) and before (black) the side-arc. The data are represented by box plots to show the median, standard deviation, and outliers over the 0.17s duration of the side-arc and the 10s leading up to the discharge. Data is shown relative to the magnetic fields generated before the side-arc. Black, blue, and red dots show the superposition of side-arc and bottom arc simulations at 0%, 26%, and 100% of the current in the side-arc, respectively.

Due to the complexity of a VAR furnace, the melt profiles to produce high quality material are developed for each furnace individually. This qualification process necessitates the expensive production and destructive analysis of ingots. The APS technology adds a new measurement that is directly related to the solidification of the ingot. Comparison between a new furnace's operations and the operation of an established furnace should add additional feedback to furnace qualification and reduce the cost of the process. This could be achieved with visual or differential comparison of APS ingot and power profiles, or by performing solidification modeling using the observed power as an input.

Analysis of the APS profiles also adds a new way to monitor the quality of ingots produced in day-to-day operations. Solidification modeling with software such as MeltFlow, BAR or SOLAR is commonly used to predict macrosegregation defects, but requires assumptions about the energy distribution input to the molten ingot, usually considered to be 2D axisymmetric and Gaussian. The APS power profiles make it possible to model the specific power distribution observed on a melt to distinguish higher quality melts or sections of ingots. In the future, this measurement may be useful to predict segregation defects in real time and modify operations to improve the resulting ingot quality.

Side-arc detection also improves VAR process monitoring by detecting safety-critical conditions which may cause a breach in the crucible. *VARmetric*TM implements side-arc detection with an array of sensors around the furnace that monitor the vertical magnetic field component. The fields measured by rings of sensors use a proprietary algorithm to monitor changes in this field during melting. This technology was tested by inducing a short-duration, controlled side-arc that carried approximately 26% of the detected arc current directly from the electrode to the crucible wall. This

side-arc detection can operate in real-time to alert operators when such conditions arise and halt operations before the furnace is compromised.

The authors would like to thank the crew at ATI Specialty Alloys & Components and Chris Lee for assistance with mounting design and installation of the *VARmetric*TM unit.

References

- [1] F. J. Zanner, "Vacuum consumable arc remelting electrode-gap control strategies based on drop short properties," *Metallurgical Transactions B- Process Metallurgy*, pp. 721-728, 1981.
- [2] R. Boxman, D. Sanders and P. Martin, *Handbook of Vacuum Arc Science & Technology: Fundamentals and Applications*, William Andrew, 1996.
- [3] P. Chapelle, H. El Mir, J. Bellot, A. Jardy, D. Ablitzer and D. Lasalmonie, "Modelling of the arc plasma behaviour in the VAR process," *Journal of materials science*, pp. 7145-7152, 2004.
- [4] F. Zanner, R. Williamson and R. Erdmann, "On the origin of defects in VAR ingots," in *Proc. International Conference on Liquid Metals*, PD Lee et al., Ed., ASM International, 2005.
- [5] R. Woodside and P. King, "Characterizing arc motion and distribution during vacuum arc remelting," in *Liquid Metals Processing Conference*, Santa Fe, NM, USA, 2009.
- [6] R. Woodside and P. King, "A measurement system for determining the positions of arcs during vacuum arc remelting," in *International Instrumentation and Measurement Technology Conference*, 2010.
- [7] R. Woodside, P. King and C. Nordlund, "Arc distribution during the vacuum arc remelting of Ti-6Al-4V," *Metallurgical and Materials Transactions B*, pp. 154-165, 2013.
- [8] R. M. Ward, B. Daniel and R. Siddall, "Ensemble arc motion and solidification during the Vacuum Arc Remelting of a nickel-based superalloy," in *Liquid Metal Processing And Casting*, Santa Fe, 2005.
- [9] M. Solar and K. Niemeyer, "Validation of an approach for detecting arc positions during vacuum arc remelting based on magnetic flux density measurements," no. <hal-01320466>, 2016.
- [10] R. L. Williamson, G. J. Shelmidine and J. P. Maroone, "Current Profiles During VAR of Ti-6Al-4V," in *Proc. International Symposium on Liquid Metal Processing and Casting*, Santa Fe, NM, USA, 2005.